COMMUNICATIONS IN COMPUTATIONAL PHYSICS
Vol. **3**, No. 1, pp. 222-249

Commun. Comput. Phys.
January 2008

Tsunami Balls: A Granular Approach to Tsunami Runup and Inundation

Steven N. Ward*and Simon Day

Institute of Geophysics and Planetary Physics, University of California, Santa Cruz, CA 95064, USA.

Received 2 January 2007; Accepted (in revised version) 6 June, 2007
Available online 14 September 2007

Abstract. This article develops a new, granular approach to tsunami runup and inundation. The small grains employed here are not fluid, but bits, or balls, of tsunami energy. By careful formulation of the ball accelerations, both wave-like and flood-like behaviors are accommodated so tsunami waves can be run seamlessly from deep water, through wave breaking, to the final surge onto shore and back again. In deep water, tsunami balls track according long wave ray theory. On land, tsunami balls behave like a water landslide. In shallow water, the balls embody both deep water and on land elements. In modeling several 2-D and 3-D cases, we find that wave breaking generally causes relative runup to increase with beach slope and wave period and decrease with input wave amplitude. Because of their highly non-linear nature, runup and inundation are best considered to be random processes rather than deterministic ones. Models and observations hint that for uniform input waves, normalized runup statistics everywhere follow a single skewed distribution with a spread between 1/2 and 2 times its mean.

AMS subject classifications: 76B15

Key words: Water wave, tsunami, run up.

1 Introduction

The thorniest issue in tsunami calculation is not deep water propagation, but rather the "first mile" where the waves generate and the "last mile" where the waves run into shallow water and then onto land. Understanding "first mile" events of tsunami birth by landslides, asteroid impacts and earthquakes is critical to fixing the intrinsic level of hazard. Understanding "last mile" events of tsunami runup and inundation is critical to mapping site-specific hazard, to the design of wave resistant structures and to the interpretation of paleotsunami deposits. This article considers those mysterious last mile events–tsunami runup and inundation.

*Corresponding author. *Email addresses:* ward@pmc.ucsc.edu (S. N. Ward), simonday_ucl@yahoo.co.uk (S. Day)

Modeling of water waves initially incident from deep water through shoaling in shallows, breaking, and finally runup onshore, must confront the changing nature of the tsunami and the movement of material and energy within. In deep water, tsunami motion is oscillatory and wave-like. The net displacement of the water mass is negligible and the velocity of energy transmission far exceeds the velocity of the individual water particles. Wave-like behavior makes for efficient propagation of tsunami over transoceanic distances. As tsunami approach shore, energy concentrates, wave heights increase to breaking, and water surges onshore. In these final flood-like stages, the net displacement of the water mass becomes large and the velocities of energy transmission and particle motion equalizes.

Most existing "last mile" approaches to wave runup and inundation (Synolakis and Bernard, 2006) employ non-linear shallow water equations and impose bore-like solutions to simulate breaking and post-breaking propagation and energy loss (Peregrine, 1966; Hibberd and Peregrine, 1979; Li and Raichlen, 2002). Others employ Boussinesq wave models augmented with extra empirical terms in the equations of motion to attempt to account for turbulent energy losses during breaking (Kennedy et al., 2000; Lynett et al., 2002). Developing numerical fluid dynamic models that span the entire 'last mile' however, has proved problematic. Special difficulties lie in quantifying the physics of turbulence, especially in proximity to the water-substrate and water-atmosphere interfaces. Those computational fluid dynamic models that do attempt to address runup and inundation in realistic three dimensional geometries are demanding computationally and susceptible to numerical instabilities (Herrmann, 2006).

This article develops a new approach to tsunami runup and inundation. The concept springs from recent work by Ward and Day, (2006) who simulated the 1980, Mt. St. Helens Washington landslide. In that simulation, granular debris raced down the mountain and then ran up and deflected from facing slopes much like a bobsled crew vying for a gold metal. The notion occurred to us that, the on-land phases of tsunami runup and inundation with all the vulgarities of deflecting and interacting flows might be modeled as a "water landslide". In debris avalanches, matter and energy do travel at the same velocity, but basal friction eventually slows and deposits solid landslide material. By eliminating basal friction, a water landslide would sooner or later drain back to the sea as does a tsunami. Although water landslides might well-emulate the on-land phase of tsunami inundation, we realized that for the approach to be useful, the deep water and runup tsunami phases have to be addressed too. The challenge posed was, "Can we formulate appropriate accelerations to carry granular water bits or 'tsunami balls' seamlessly from deep water, to breaking, onto land, and back again?"

2 Tsunami balls

We intend to simulate near shore tsunami wave propagation, runup, and inundation by tracking accelerating tsunami balls. Because the physical behavior of water motion takes

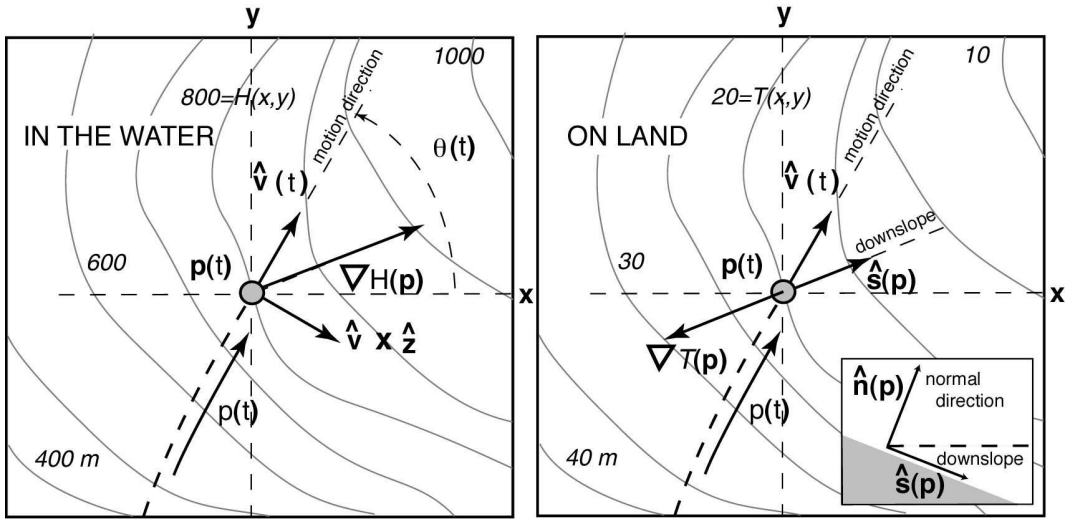

Figure 1: Geometry for accelerating tsunami balls. Quantities are measured as a vector function of time $\mathbf{p}=\mathbf{p}(t)$ or as a scalar function of distance along the path $p=p(t)$. (Left) In water, tsunami balls will speed or slow depending on the sign of $\hat{\mathbf{v}}(t)\bullet\nabla H(\mathbf{p}(t))$ and always accelerate toward shallow water, increasing or decreasing the azimuth $\Theta(t)$ of the path depending on the sign of $(\hat{\mathbf{v}}(t)\times\hat{\mathbf{z}})\bullet\nabla H(\mathbf{p}(t))$. (Right) On land, we introduce the unit upward normal to the topographic surface $\hat{\mathbf{n}}$ and the down slope direction $\hat{\mathbf{s}}$ (insert) Tsunami balls on land always accelerate down slope.

different forms at different stages in this sequence, the accelerations take three forms–deep water, near shore/breaking and onshore–depending upon the ball's current location. Fig. 1 sets the stage for tsunami ball theory with $\hat{\mathbf{x}}$ and $\hat{\mathbf{y}}$ directions being east and north in the horizontal plane and $\hat{\mathbf{z}}$ being up so $\mathbf{g}=-g\hat{\mathbf{z}}$. Let $T(x,y)$ be topographic height measured positive upward from still water. Over water $T(x,y)=-H(x,y)$, where $H(x,y)>0$ is the ocean depth.

2.1 Deep water accelerations

In water of depth greater A_{crit} (to be specified later) we would like tsunami balls to mimic long water waves. Accordingly, we assume that deep-water tsunami balls at position $\mathbf{p}(t)$ that have velocity $\mathbf{v}(t)=v(t)\hat{\mathbf{v}}(t)$ in the $\hat{\mathbf{x}}$-$\hat{\mathbf{y}}$ plane accelerate according to

$$\begin{aligned}&\mathbf{a}_{dw}(t)=(g/2)\hat{\mathbf{v}}(t)\hat{\mathbf{v}}(t)\bullet\nabla H(\mathbf{p}(t))-(\hat{\mathbf{v}}(t)\times\hat{\mathbf{z}})v(t)R(t),\\&R(t)=(g/2v(t))(\hat{\mathbf{v}}(t)\times\hat{\mathbf{z}})\bullet\nabla H(\mathbf{p}(t)).\end{aligned}\tag{2.1}$$

The first term in (2.1) acts in the direction of motion $\hat{\mathbf{v}}$ and speeds or slows the tsunami ball. The second term in (2.1) acts perpendicular to the direction of motion and deflects the ball's path in the horizontal plane without changing its speed. $R(t)$ is the rotation rate of the ball's direction.

Eq. (2.1) is not meant to represent an equation of motion in the usual sense of conservation of momentum; rather, it has been devised to impart on the tsunami balls certain

shallow water wave properties. For instance, if scalar $p=p(t)$ measures distance along a tsunami ball path, then $\hat{\mathbf{v}}(t)\bullet\nabla H(\mathbf{p}(t))=\partial H(p)/\partial p$ and the first term in (2.1) is

$$\begin{aligned} a(t)&=\partial v(t)/\partial t=(\partial p/\partial t)(\partial v(p)/\partial p)\\ &=v(p)(\partial v(p)/\partial p)=(g/2)\partial H(p)/\partial p, \end{aligned} \tag{2.2}$$

where $H(p)$ is the water depth. It is easy to show that $v(p)=\sqrt{gH(p)}$ satisfies (2.2)

$$(\partial v(p)/\partial p)=(g/2v(p))\partial H(p)/\partial p$$

so once a tsunami ball is started in any direction with $v_o=\sqrt{gH_o}$, the first term in (2.1) assures that it will accelerate to keep the long wave tsunami speed of $v(p)=\sqrt{gH(p)}$ everywhere along its path. Additionally, because

$$v(p)=\sqrt{gH(p)},\quad \nabla v(\mathbf{p})=(g/2v(\mathbf{p}))\nabla H(\mathbf{p}),$$

the second term in (2.1) is

$$\mathbf{a}(t)=v(p)(\partial\mathbf{v}(p)/\partial p)=-(\hat{\mathbf{v}}(t)\times\hat{\mathbf{z}})(g/2)(\hat{\mathbf{v}}(t)\times\hat{\mathbf{z}})\bullet\nabla H(\mathbf{p}(t))$$

or

$$(\partial\mathbf{v}(p)/\partial p)=-(\hat{\mathbf{v}}(p)\times\hat{\mathbf{z}})(\hat{\mathbf{v}}(p)\times\hat{\mathbf{z}})\bullet\nabla v(\mathbf{p}). \tag{2.3}$$

Because this acceleration only changes the direction of $\mathbf{v}(p)$ not its magnitude, (2.3) is

$$\partial\Theta(p)/\partial p=\frac{(\hat{\mathbf{v}}(p)\times\hat{\mathbf{z}})\bullet\nabla v(\mathbf{p})}{v(p)}, \tag{2.4}$$

where $\Theta(p)$ is the angle of the ball's direction measured from $\hat{\mathbf{x}}$ to $\hat{\mathbf{y}}$. Eq. (2.4) is just the standard formula for tracing tsunami rays in a plane (Chou, 1970). Tsunami balls accelerating according to (2.1) maintain long wave tsunami speeds and track tsunami paths as given by ray theory.

Energy balls

In deep water, tsunami are wave-like in that tsunami energy travels at $v(p)=\sqrt{gH(p)}$ and not the water mass itself. Accordingly, we consider the tsunami balls to possess a fixed energy E_o. At any location, the amplitude of the tsunami wave above still water $A(\mathbf{p})$ relates to the number density $\sigma(\mathbf{p})$ [m^{-2} units] of tsunami balls in the $\hat{\mathbf{x}}$-$\hat{\mathbf{y}}$ plane by

$$A(\mathbf{p})=\left[\frac{\sigma(\mathbf{p})E_0}{\rho g}\right]^{1/2}, \tag{2.5}$$

where ρ is the density of water. We take the square root in (2.5) to be positive, although the concept of wave troughs being represented by the negative sign choice has been considered.

Imagine now, shooting off one tsunami ball per second governed by (2.1) with $v(\mathbf{p}_o)=\sqrt{gH(\mathbf{p}_o)}$ in some fixed direction. Because all the balls follow the same path at the same rate and can't stop, for any other point along the path the balls must also pass one per second. Energy flux is conserved. Ball speeds change along the path however, so energy density $\rho(\mathbf{p})E_o$ and wave amplitude (2.5) will change. At the start of the path $\sigma(\mathbf{p}_o)E_o=E_o/[v(\mathbf{p}_o)\times$ (1s) (1m)] and somewhere else along the path $\sigma(\mathbf{p}_1)E_o=E_o/[v(\mathbf{p}_1)\times$ (1s) (1m)]. From (2.5), tsunami amplitude at $\mathbf{p}_1$ relates to amplitude at $\mathbf{p}_o$ by

$$A(\mathbf{p}_1)=A(\mathbf{p}_o)\left[\frac{v(\mathbf{p}_o)}{v(\mathbf{p}_1)}\right]^{1/2}=A(\mathbf{p}_o)\left[\frac{H_o}{H_1}\right]^{1/4}. \tag{2.6}$$

(2.6) is the shoaling relation (Green's Law) of linear, long wave tsunami wave theory.

Recapitulation of deep water behaviors

Tsunami energy balls accelerating by (2.1): (a) keep long wave tsunami speeds, if started at long wave speeds; (b) follow long wave tsunami ray paths; (c) conserve energy flux; and (d) obey the long wave shoaling relation (Green's Law).

2.2 On land accelerations

On land, tsunami are not wave-like but flood-like–the distinction being that in the latter, energy and mass move at the same speed. On land, we assume initially that the tsunami balls accelerate according to

$$\mathbf{a}_l(t)=[\mathbf{g}\bullet\hat{\mathbf{s}}(\mathbf{p}(t))]\hat{\mathbf{s}}(\mathbf{p}(t))=\mathbf{g}-[\mathbf{g}\bullet\hat{\mathbf{n}}(\mathbf{p}(t))]\hat{\mathbf{n}}(\mathbf{p}(t)). \tag{2.7}$$

Unit vectors $\hat{\mathbf{n}}(\mathbf{p})$ and $\hat{\mathbf{s}}(\mathbf{p})$ are the upward unit normal and down slope directions of the topography $T(x,y)$ at $\mathbf{p}$ (Fig. 1, right). You calculate these directions from $T(x,y)$ from

$$\hat{\mathbf{n}}(\mathbf{p})=\frac{-\nabla T(x,y)+\hat{\mathbf{z}}}{\sqrt{1+\nabla T(x,y)\bullet\nabla T(x,y)}}, \tag{2.8}$$

$$\hat{\mathbf{s}}(\mathbf{p})=\frac{-\hat{\mathbf{z}}+(\hat{\mathbf{z}}\bullet\hat{\mathbf{n}}(\mathbf{p}))\hat{\mathbf{n}}(\mathbf{p})}{\sqrt{1-(\hat{\mathbf{z}}\bullet\hat{\mathbf{n}}(\mathbf{p}))^2}}. \tag{2.9}$$

Unlike (2.1), (2.7) is meant to be a real equation of motion. Acceleration (2.7) is simply the component of gravity resolved in the downslope direction of topography $T(x,y)$. Because $\mathbf{g}\bullet\hat{\mathbf{s}}(\mathbf{p}(t))\geq 0$, (2.7) always accelerates on-land tsunami balls downhill, back toward the ocean.

2.3 Self-topography

Ward and Day (2006) used Eq. (2.7), with two friction terms, to model the Mt. St. Helen's debris avalanche. For water flows, additional self-topographic forces are desirable to

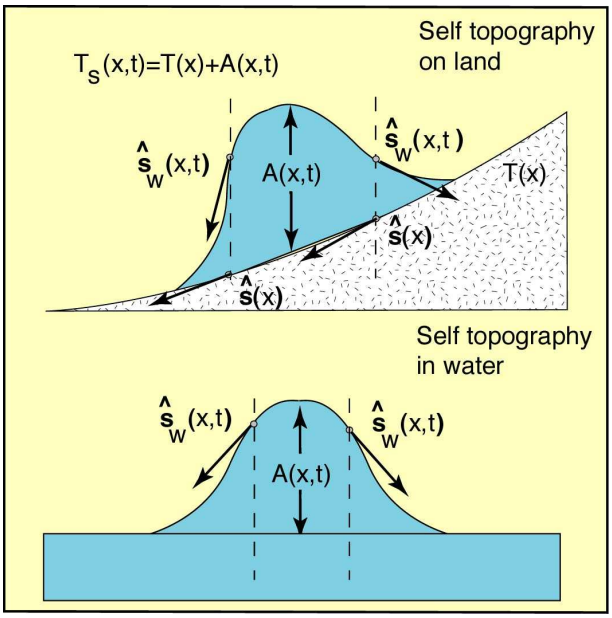

Figure 2: (Top) Self-topography on land. Downslope directions are not evaluated on the topographic surface $T(x)$, but rather on $T(x)+A(x,t)$, the on-land surface of the water. (Bottom) Self topography in shallow water, downslope directions are evaluated on $A(x,t)$. Wherever applied, self-topography pulls water piles apart.

mimic flooding. To include self-topography, replace land topography $T(x,y)$ in (2.8) and (2.9) with

$$T_S(x,y,t) = T(x,y) + A(x,y,t),$$

where $A(x,y,t)$ is the water height at (x,y) at time t. $A(x,y,t)$ relates to the number density of tsunami balls $\sigma(x,y,t)$ that happen to be at that position at that time through (2.5). Eq. (2.7) now resolves the acceleration of gravity in the downslope direction of topography plus the water height (Fig. 2, top). $T_S(x,y,t)$ of course, describes the on-land water surface itself. Self-topography drives piles of water apart by accelerating tsunami balls on opposing slopes outward (Fig. 2, top). Self-topography complicates the calculation in that (2.8) and (2.9) become time-dependent.

2.4 Shallow water/breaking accelerations

If tsunami balls followed Eq. (2.1) all the way to shore, they would come to a complete stop where $H = 0$ and never make it onto land. Clearly, between the deep water wave-like zone (2.1) and the on-land flood-like zone (2.7), tsunami transition. In shallow water where wave heights surpass A_{crit}, we adopt a transitional shallow water acceleration

$$\mathbf{a}_{sw}(t) = \mathbf{a}_{dw}(t) + (1/2)[\mathbf{g} \bullet \hat{\mathbf{s}}_w(\mathbf{p}(t))]\hat{\mathbf{s}}_w(\mathbf{p}(t)), \tag{2.10}$$

where

$$\hat{\mathbf{n}}_w(\mathbf{p},t)=\frac{-\nabla W(x,y,t)+\hat{\mathbf{z}}}{\sqrt{1+\nabla W(x,y,t)\bullet\nabla W(x,y,t)}}, \tag{2.11}$$

$$\mathbf{s}_w(\mathbf{p},t)=\frac{-\hat{\mathbf{z}}+(\hat{\mathbf{z}}\bullet\hat{\mathbf{n}}_w(\mathbf{p},t))\hat{\mathbf{n}}_w(\mathbf{p},t)}{\sqrt{1-(\hat{\mathbf{z}}\bullet\hat{\mathbf{n}}_w(\mathbf{p},t))^2}}. \tag{2.12}$$

Appropriately, (2.10) blends on land and deep water behaviors. The first term replicates the deep water acceleration (2.1). The second term is one-half of (2.7) including only the self-topographic forces imparted by slopes of the water surface (Fig. 2, bottom). Unlike (2.7), acceleration (2.10) acts only on tsunami balls in water so land topography $T(x,y)$ need not be included. Self-topographic forces imposed in shallow water are fundamental to runup and inundation. Self-topographic forces accelerate the leading edge of tsunami onto land despite the efforts of long wave forces (2.1) to stop it at the beach. Self-topographic forces also act to turn back trailing edges of tsunami prior to reaching the beach. Wherever applied, self-topography flattens water piles. In water shallower than A_{crit}, waves subject to (2.10) are in fact, breaking.

2.5 Friction

Following Ward and Day (2006) we introduce a dynamic drag friction

$$\mathbf{a}_F(t)=-\nu[v^2(\mathbf{p}(t))]\hat{\mathbf{v}}(\mathbf{p}(t)), \tag{2.13}$$

where $\nu=0.001/m$ is a small, but adjustable coefficient. Frictional accelerations always act in opposition to velocity. Dynamic drag (2.13) intends to represent an actual energy loss but it also helps to stabilize numerical realizations, particularly in restraining balls sent careening by errant evaluation of topographic slope. We add (2.13) to accelerations (2.7) for those tsunami balls on land and also to accelerations (2.1) for any deep water balls that, for numerical reasons, have gone hyperspeed $v(p)>\sqrt{gH(p)}$.

3 Calculations in two dimensions

3.1 Simple beach

To illustrate the tsunami ball approach to runup and inundation, consider a two-dimensional coastline with topography

$$\begin{aligned} T(x)&=-H_0(1-e^{-x\tan(\beta)/H_0}):\ x>0,\\ T(x)&=-x\tan(\beta):\ x<0, \end{aligned} \tag{3.1}$$

where H_0 is the deep water depth and β gauges the slope at the beach (Fig. 3). Onto this shore, tsunami balls will be sent in from the right. In Fig. 3, the line labeled $A_G(x)$ traces

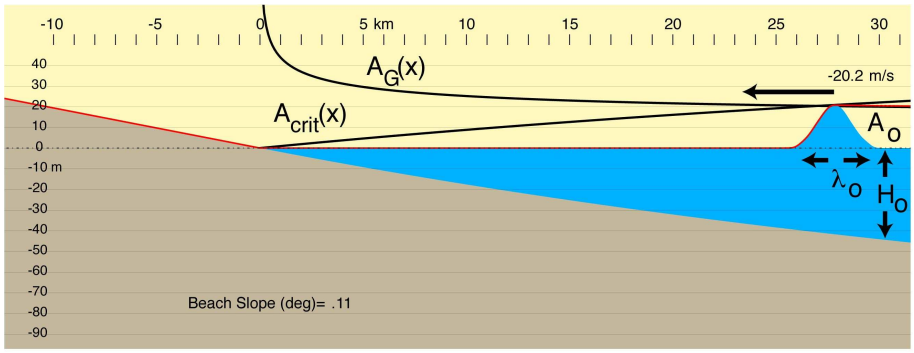

Figure 3: Geometry for two-dimensional runup and inundation. Wave pulses of different initial amplitude and wavelength run to shore from the right. Topography (brown) follows Eq. (3.1). The two black lines trace Greens Law (3.2) and the proposed value of A_{crit}. Where wave height is less than A_{crit}, tsunami balls accelerate according to (2.1). When wave height exceeds A_{crit}, accelerations revert to (2.10). Tsunami balls on land ($x<0$) accelerate using (2.7).

Green's Law

$$A_G(x) = A_0 \left[\frac{H_0}{H(x)} \right]^{1/4}, \tag{3.2}$$

with A_0 being the wave amplitude in water depth H_0, and $H(x)$ a water depth closer to shore. We have established that waves of tsunami balls following deep water accelerations (2.1) grow according to this curve. $A_G(x)$ runs to infinity at the shore and belies the failure of (2.1) to take tsunami close to the beach. The line $A_{crit}(x)$ in Fig. 3 marks the critical wave height where tsunami balls transition from accelerations (2.1) to (2.10). Wave shoaling experiments (Le Mehaute and Wang, 1996) suggest that water waves deviate from Green's Law when their amplitude exceeds 3/4 to 5/4 of the local water depth $H(x)$. In this article, we select a simple wave amplitude-based breaking criterion

$$A_{crit}(x) = \frac{H(x)}{2} \tag{3.3}$$

to define the transition. (Coefficients different from 1/2 or other wave slope or bottom slope-based breaking criteria might be considered in the future.) Where $A_G(x)$ and $A_{crit}(x)$ cross, waves may, if they are large enough, take on shallow water behavior (2.10). Recall that (2.10), unlike (2.1) includes accelerations due to self topography. Self-topography spreads the wave and cuts its height in a breaking action. The consequences of breaking depend upon the length of time that the force acts (proportional to the distance offshore that lines $A_G(x)$ and $A_{crit}(x)$ cross) and the strength of the force (proportional to the steepness of the wave). Not surprisingly, breaking actions are complex, being functionals of ocean depth along the wave path, wave period, wave amplitude and wave shape.

The following two-dimensional experiments distribute 16,000 tsunami balls with a Gaussian number density $\sigma(\mathbf{p})$ just off the right side of the figures. The width of the

Gaussian distribution varies in the different experiments to simulate waves of different periods. (In this paper, the period of a single wave crest is just the time it takes to pass a point.) We select tsunami ball energy E_0 to give the desired initial wave height as computed by (2.5). The i-th ball starts with a leftward velocity of $\sqrt{gh(x_i^o)}$ where x_i^o is its initial position. Once started with these initial conditions, Eqs. (2.1), (2.7), (2.10) and (2.13) guide the evolution of the wave for the remainder of the experiment. Note that the rotation term $R(t)$ vanishes in two-dimensions.

3.2 Shallow slope–short waves

To construct a representative coastal section, let $H_0=100$m and $\beta=0.11^\circ$ (1:520 slope) in (3.1). The first example (Fig. 4) sends in a single pulse of 50s duration and 20m height. At 50s, the period of this pulse exceeds the 10-15s periods of wind driven waves. Tsunami of 50s period might be sourced from small volume landslides or from impacts of asteroids of about 100m diameter. With 20m amplitude, this steeply-sided wave might be representative of the latter.

At first (Frames 1 and 2, Fig. 4), tsunami balls obey deep water accelerations and wave amplitude follows Greens law (3.2). Near x=25km wave amplitude first tops $A_{crit}(x)$ and the self-topographic forces turn on and start to shave and spread the pulse. As pictured in Fig. 2b (bottom), self-topography acts to accelerate material on the leading edge of the wave toward shore and material on the trailing edge back to sea. As a consequence, after continued contact with $A_{crit}(x)$, the single pulse begins to tear apart. For a periods of time and portions of broken wave however, amplitudes fall below $A_{crit}(x)$ and (2.1) again governs the tsunami balls temporarily (Frame 3). Wave breaking is not necessarily continuous. As the wave approaches shore, breaking eventually knocks down the single pulse into several (Frames 5 and 6). Frame 7 shows maximum inundation of 8.7m - considerably less than the 20m input height. Breaking across shallow seas takes a heavy toll on steep sided, short wavelength tsunami. Runup amplification R/A_0 (the ratio of initial height to runup height) in this instance is just 0.43.

The red line in Fig. 4 plots the peak value of wave height offshore, or peak flow depth plus topography onshore. Due to interfering in- and out-flows, peak runup might be found anywhere along the beach, not always at the point of maximum incursion. Wave breaking and wave interference incorporate highly non-linear processes. Minor differences in initial conditions spawn variations in runup even under idealized conditions. In real world applications where topographic variations are stronger and poorly known, "random" elements in runup increase (Section 4).

The reader should be aware that the runup and inundation figures in this article (plus others) are accompanied by Quicktime movies. The movies reveal aspects of runup, breaking and inundation far better than the still frames. To view the Quicktime movie for Fig. 4 click RU(50s-20m-0.11).mov (Note– prefix "http://es.ucsc.edu/∼ward/" has been dropped from all of the hyperlinks in the text).

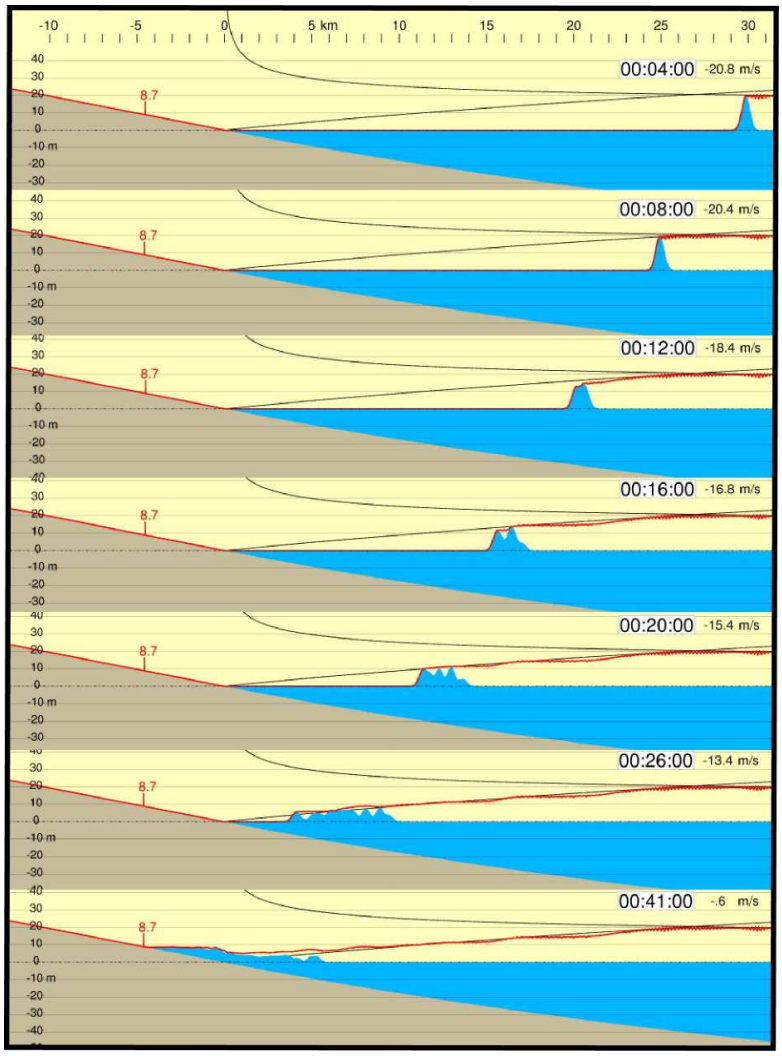

Figure 4: Runup and inundation of a 20m high, 50s duration wave. Large amplitude, short wavelength tsunami waves may break far offshore, reducing their runup potential.

3.3 Shallow slope–intermediate waves

Fig. 5 illustrates runup and inundation of a 20m high, 180s period wave pulse. Tsunami of 180s period might be sourced from moderate volume landslides or from impacts of asteroids of about 2000m diameter. A similar sequence of events affect the 180s pulse as did the 50s pulse in Fig. 4. The larger-dimensioned 180s wave pulse however, resists disruption more than shorter length 50s waves. Still, breaking takes its tax and peak runup from the 20m wave reached only 12.6m. Runup amplification increased to 0.63 from 0.43 for the 50s pulse, but R/H_0 remains less than one. The Quicktime movie for Fig. 5 can be seen by clicking RU(180s-20m-0.11).mov

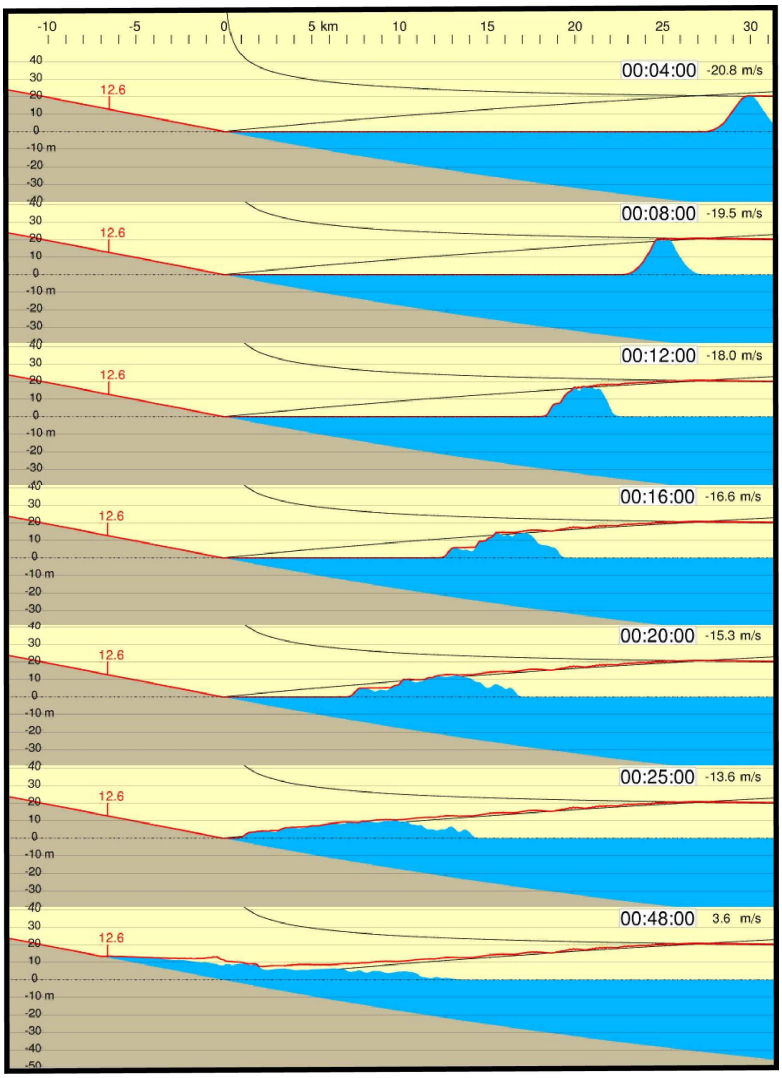

Figure 5: Runup and inundation of a 20m high, 180s duration wave. A 180s wave period might be generated from moderate volume landslides or from impacts of large asteroids.

3.4 Shallow slope–long waves

Fig. 6 illustrates runup and inundation of a 20m high, 1200s period wave pulse. Waves with 10 to 20 minute period characterize tsunami generated by subduction zone earthquakes or very large landslides. Breaking affects waves of this dimension differently. Contact with A_{crit} shaves wave height (Panels 2-5, Fig. 6) but otherwise only slightly disrupts its progress. A long period tsunami acts like a 100 car coal train–even after brakes are applied, a long time elapses before the train slows. Note the bore-like steep front that develops as the wave approaches and onsets land (Panels 4-6). Waves of this length raise

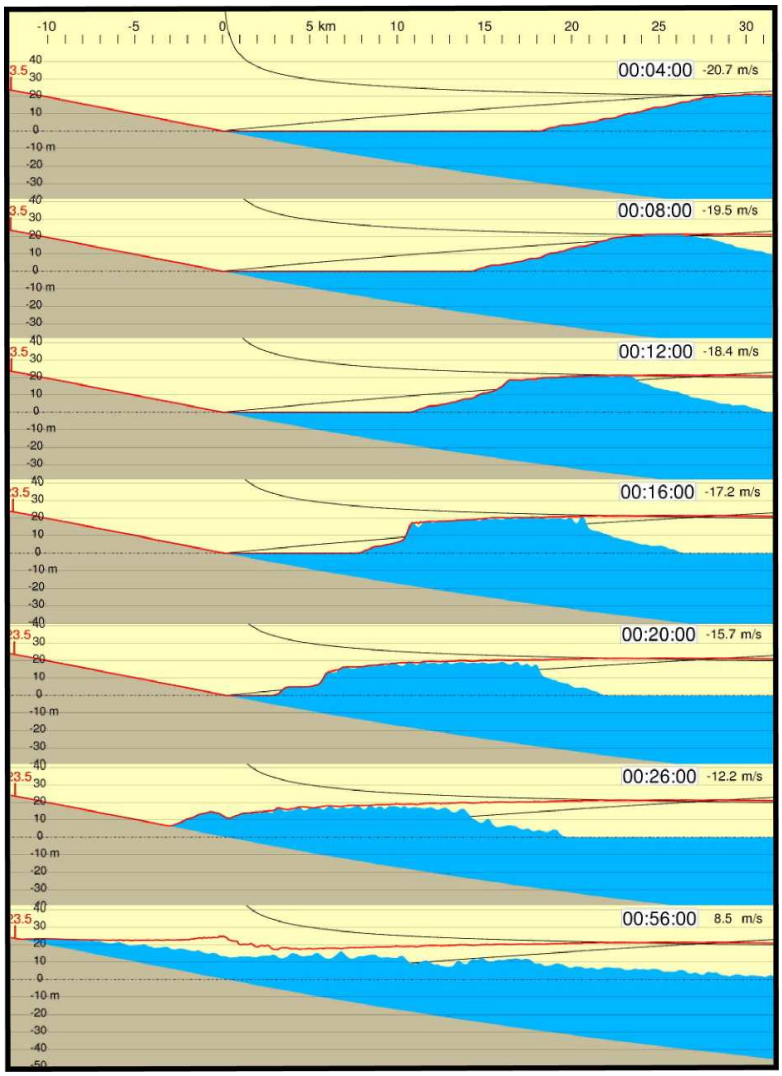

Figure 6: Runup and inundation of a 20m high, 1200s duration wave. Typical of earthquake tsunami, long waves like this are difficult to stop.

flood-like inundations lasting many tens of minutes. Peak runup now reaches 23.5m and R/H_0 increased to 1.17 from 0.63 for the 180s pulse. Play the Quicktime movie for Fig. 6 here RU(1200s-20m-0.11).mov

Figs. 4-6 argue that for tsunami pulses of fixed height running onto shallow beaches, breaking impacts longer period waves less than shorter period ones. A sensible proposal for sure, but it would be useful to consult laboratory results for comparison and calibration. Unfortunately, no experiment that we are aware of employs slopes as shallow (1:500) nor waves as long ($\lambda_0 = 10-500H_0$). In fact, rarely do wave tanks slope shallower than 1:50 or do input wavelengths exceed a few times H_0. The need to extrapolate labo-

ratory experiments to 'outside' scales has always loaded heavy uncertainly onto tsunami research. (See Appendix A).

3.5 Steeper slope–long waves

Here, we increase beach slope to 0.5°. A 1:114 incline is moderately steep for real world situations but it still falls at the shallowest fringe of lab experiments. For a fixed wave height, steeper slopes bring the crossover between $A_G(x)$ and $A_{crit}(x)$ closer to shore. Generally, the closer that the cross over point approaches shore, the shorter the time that breaking operates on the wave and the greater the final runup surge. In Fig. 7, the wave virtually contracts the beach before breaking criterion (3.3) kicks in (Panel 4). Collapse of the steep front face (Panel 5) forces runup to 40.5m–double that of Fig. 6. The Quicktime movie for Fig. 7 can be seen by clicking RU(1200s-20m-0.5).mov

3.6 Offshore pile-ups and reverse breakers

Curiously in these calculations, only a fraction of the tsunami balls sent toward land cross the coastline. Many balls get "ponded" behind the wave's front piling on the beach. The water pile-up is analogous to traffic jamming at an obstruction, or sports fans queuing at turnstiles. Water in the rear of the wave actually turns back in reverse facing, then reverse traveling breakers even before peak runup (Panels 4-6, Fig. 6 and Panels 6-7, Fig. 7). Few observations of near shore pile-up exist because most tsunami are witnessed from land where attention focuses upon onshore events. However, photos taken from yachts anchored in 10 to 15m of water (about twice tsunami amplitude) offshore Phi Phi Island Thailand during the December 26th 2004 tsunami document both the near shore water pile-up and steep off shore-directed waves. A series of digital, time-stamped photographs http://www.yachtaragorn.com/Thailand.htm provide flow indicators in the seaward-pointing bows of other anchored yachts and the bow waves generated by the rapid motion of the water (We reproduce selected photos in Fig. 16, Appendix B). During the initial period of onshore-directed flow in the 2004 tsunami, the photographs show the development of a steep, breaking front at the seaward side of a near shore pile-up of water several meters high. Over a period of a few minutes, while the overall flow direction was still shoreward, this front developed into multiple reverse traveling breakers with lengths several times that of the yachts. One of the boats reported to have grounded on a patch reef during the initial withdrawal but, as if riding on the pile thereafter, it gave no report of grounding in later wave troughs.

The yacht Mercator, anchored off Nai Harn beach, Phuket provides further evidence of the nearshore pile-up (See Fig. 17, Appendix B). The yacht's echo sounder http://www.zeilen.com/publish/article_1659.shtml records: (a) pre-tsunami water depth of 11 to 12m; (b) the initial drawdown to a minimum water depth of 8m; (c) three following crests with maximum water depths of 15, 13 and 17 meters at intervals of around 13 minutes. At no time between these crests did soundings drop below 11m.

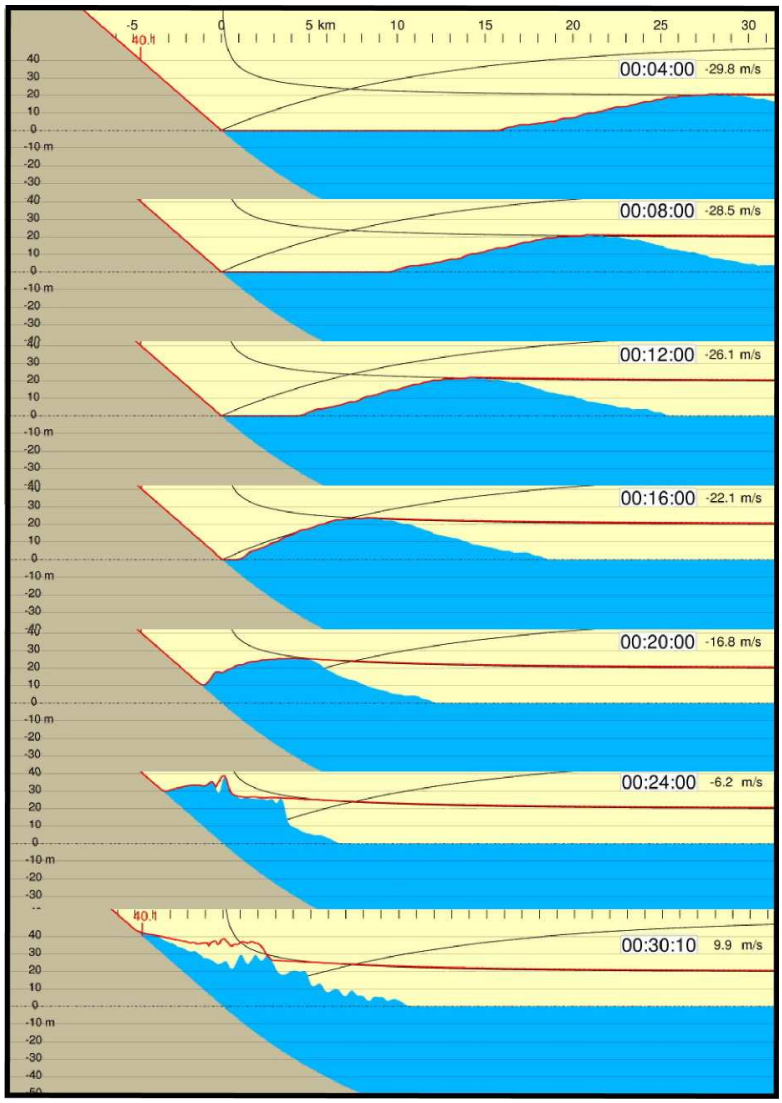

Figure 7: Runup and inundation of a 20m high, 1200s duration wave on a steep 0.5° beach. On steep beaches breaking has little time to operate so runup amplifications are large. Note the formation of reverse breakers in Panels 5-6.

Thus, for the first hour of the tsunami, the mean water depth offshore was significantly greater (by ∼1.5m) than prior to the tsunami, again indicating a persistent pile-up in shallow water.

3.7 Conclusions about single wave runup in two-dimensions

Fig. 8 summarizes runup results for the examples shown and several others. The figure plots runup amplification (R/A_0) versus input wave amplitude normalized by the initial

50m, 95m and 100m water depths of the experiments. (For other starting conditions A_0' and H_0' replace A_0 on both axes by $A_0'[H_0'/\mathrm{H}_0]^{1/4}$.) Colors red, orange and green display (R/A_0) for 1200, 180 and 50s. In virtually all cases, runup amplification increases with wave period and decreases with initial wave amplitude. Simply put, breaking more strongly affects steeper waves than flatter ones.

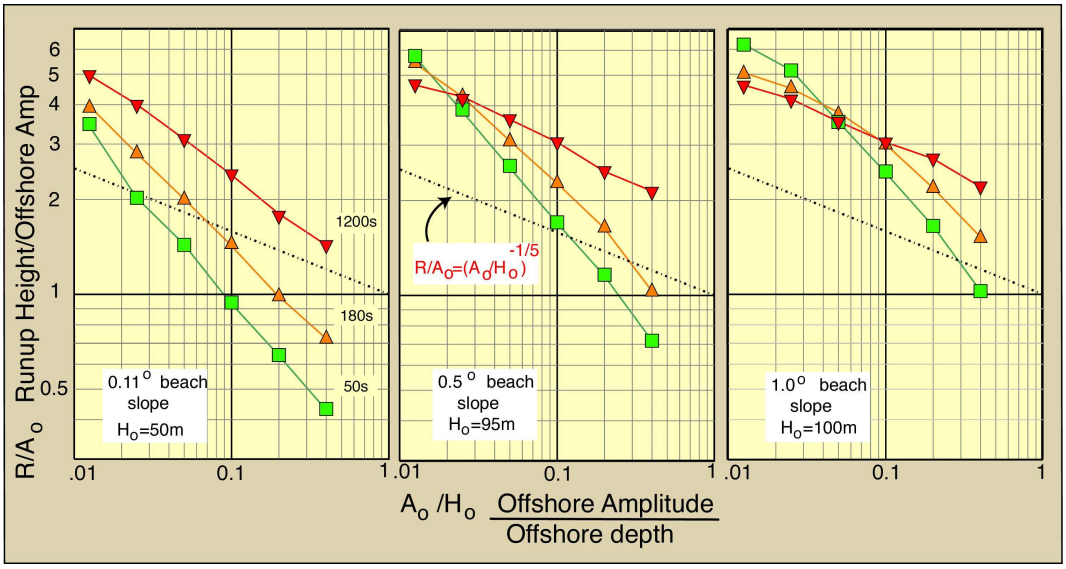

Figure 8: Summary of two-dimensional single wave runup experiments for fixed H_0. (Left) 0.11° slope 1:520, $H_0=50$m. (Middle) 0.5° slope 1:114, $H_0=95$m. (Right) 1° slope 1:57, $H_0=100$m. Red, Orange and Green curves correspond to input waves of 1200s, 180s, and 50s period. Longer period waves on steeper beaches generally produce larger runup relative to their input amplitudes.

The dashed line in the Fig. 8 plots

$$R/H_0=(A_0/H_0)^{0.8} \text{ or } R/A_0=(A_0/H_0)^{-0.2}, \quad A_0<H_0\ll\lambda_0. \tag{3.4}$$

Ward (2002) and Chesley and Ward (2006) used (3.4) as a universal runup formula in situations where no case-specific information was available. They realized that Eq. (3.4), being independent of wave period or beach slope, can not hold everywhere (See Appendix A). Eq. (3.4) always returns $R/A_0>1$, but we have already seen (e.g. Figs. 3 and 4) that $R/A_0<1$ when breaking is strong (large, short period waves on shallow beaches). On the other hand, Fig. 8 proposes that (3.4) understates runup in weakly breaking cases, so the formula might represent a decent compromise, given no other information.

Empirical runup formulas like (3.4) derive from solitary wave experiments that ignore "set up" (see below). Such formulas, even more complex ones (See Appendix A), broad brush reality. Moreover, randomness in runup may swamp differences due to beach slope, wave period etc. In Section 5, we argue that run up is more practically viewed as a random variable. At best, empirical runup laws might characterize the mean of its distribution.

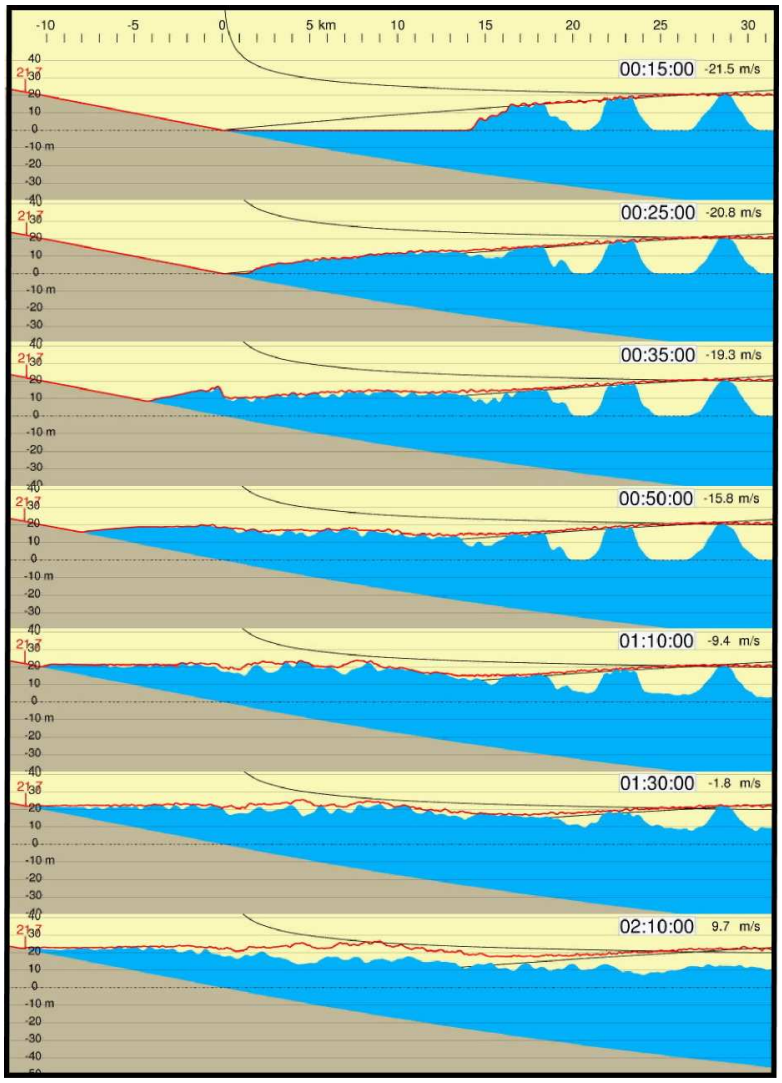

Figure 9: Runup and inundation of a set of twenty, 20m high, 180s duration waves. Note the slow and persistent flooding of the land due to set up. Set up may be more important to certain tsunami hazards than run up.

3.8 Shallow beach–sets of waves

Run up gets most of the attention in tsunami experiments, but tsunami hazard stems not just from runup height, but run in distance too–that is, how far water penetrates inland. Run in depends on the steepness of the beach and the size and period of the tsunami. Run in also varies with the number of impinging waves.

Fig. 9 samples runup and inundation from a set of twenty 180s wave pulses like Fig. 5, sent into shore at five minute intervals. Near the coast, it takes time for the outflow of water to match the influx of water carried by the waves. We discussed the pile-up of

single waves in the section above. Now, with multiple waves, the pile-up amplifies in size and duration and the total effect is called "set up". Set up shows largely as a slow flooding of the land. Set up harks to storm surge, but set up is not driven by atmospheric pressure or wind. The duration of set up induced flooding spans not just the duration of one wave, but the duration of the entire wave train. This might mean hours. The single wave (Fig. 5) ran up 13m and ran in 7km whereas the wave set in Fig. 9 ran up 22m and ran in 12km. Preliminary experiments suggest that in the presence of set up, long wave trains produce relative runups $R/A_0 \sim 1$ [$A_0 < H_0/2$; $H_0 \sim 100$m] independent of beach slope or wave period. The additional run-in distance from a set of small waves might be more hazardous in terms of the number of folks affected than a single wave of higher run up but smaller run in. Set up is especially relevant to impact- or landslide-generated tsunami because these entail long trains of waves. Click here RU(180s-20m-0.11)set.mov for a Quicktime version of Fig. 9.

4 Calculations in three dimensions

The true beauty of tsunami balls show in three-dimensions where rotation of ball trajectories toward shallower water come into play. Rotation of wave fronts obliquely approaching shore to a more normal incidence and refraction of energy around headlands are common manifestations. Strong bending and repeated reflections from land also trap wave energy in offshore shallows.

4.1 Babi Island

Consider first, an island with circular symmetry (Fig. 10) modeled after Babi Island, Indonesia. In the Flores tsunami of 1992, waves refracted around the conical island volcano and converged on its lee side. Exceptionally high runups there destroyed two villages that, at first thought, might have been protected by the island. Briggs et al. (1994, 1995), Liu et al. (1995), and Titov and Synolakis (1995, 1998) adopted Babi Island as an experimental and computational benchmark.

Our simulation adopts an ocean depth of the form

$$h(r) = 310m - 360me^{-r^2/30{,}000}, \tag{4.1}$$

where r measures distance from the Island's center in meters. Eq. (4.1) generates an island 20km wide with a slope at the beach of about 0.5°. Toward this target we send 50,000 tsunami balls in an initial uniform 4m high, 35km wide (600s period) wave as pictured in the upper left panel of Fig. 10. The i-th ball starts with a rightward velocity of $\sqrt{gH(\mathbf{r}_0^i)}$ where $\mathbf{r}_0^i$ is its initial position. What run up predictions do the two dimensional results offer? Green's Law (3.2) says that a wave starting at 310m depth should have amplitude $4(310/95)^{0.25} = 5.4$m at 95 m. Given an offshore height to offshore depth ratio there of

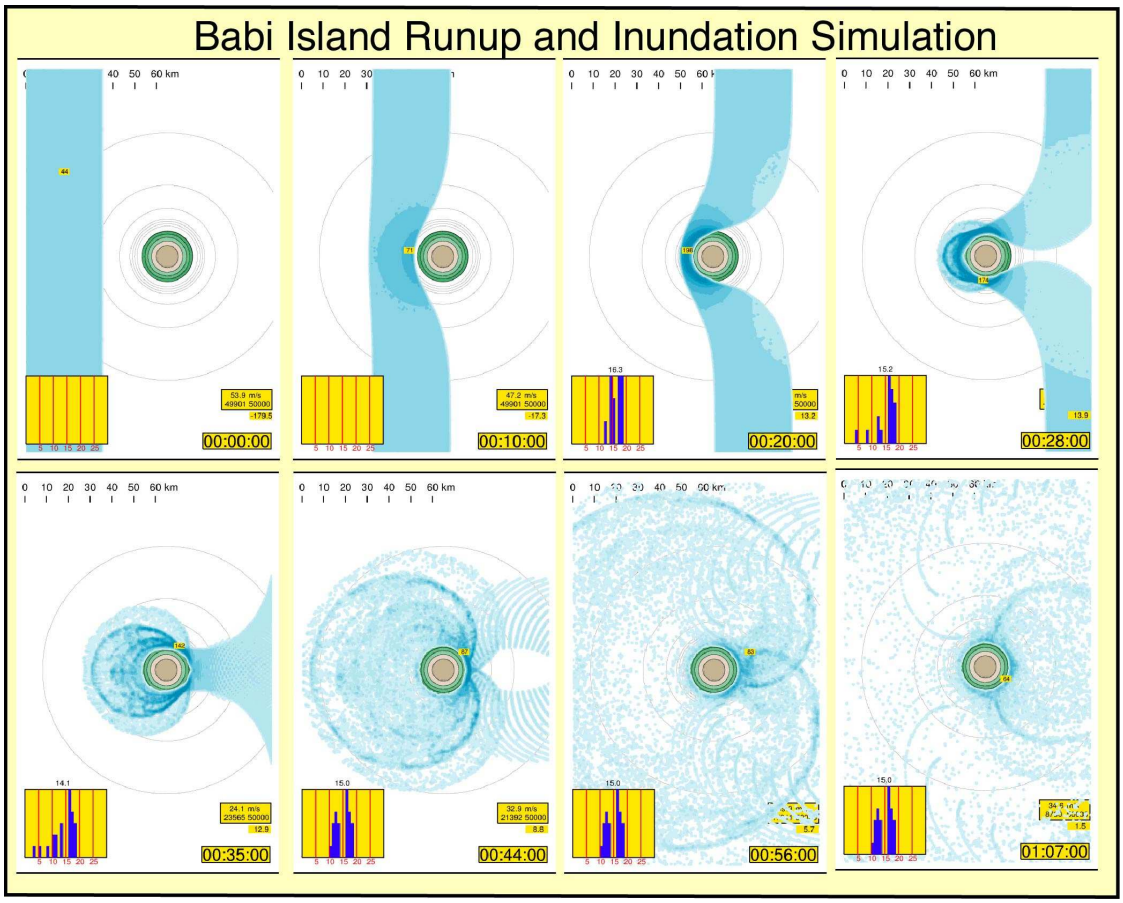

Figure 10: Application of tsunami ball theory to Babi Island runup and inundation. Note the focussing and compression of the wave at the Island front and the wrap-around at the Island back. The yellow box at lower left shows the statistical distribution of runup heights along the coast.

$\sim$0.06, a beach slope of $\sim 0.5°$, and a period of 600s, the center frame of Fig. 8 predicts that on a plane beach, the wave should run up $\sim$3.1 times its height at 95m depth, or 16.7m.

Panels 1-4 of Fig. 10 illustrate the sequence of wave compression, inundation, and reflection off Babi Island in a circular front. Panels 5-7 show wave wrap-around. Runups on the exposed front side of this island reached 16-18m, a bit more than expected for a plane beach, but refraction focuses energy toward the nose of the island. Runups on the lee of the island reached 11-12m–less than the front side, but still significant. In the mean, the 16.7m prediction holds well. Panel 8 shows multiply refracted/reflected waves starting the second orbit of the Island. A few tsunami balls get trapped for hours. Movies of Fig. 10 are here Babi.mov and Babi-num.mov. The second of these samples runup heights and locations.

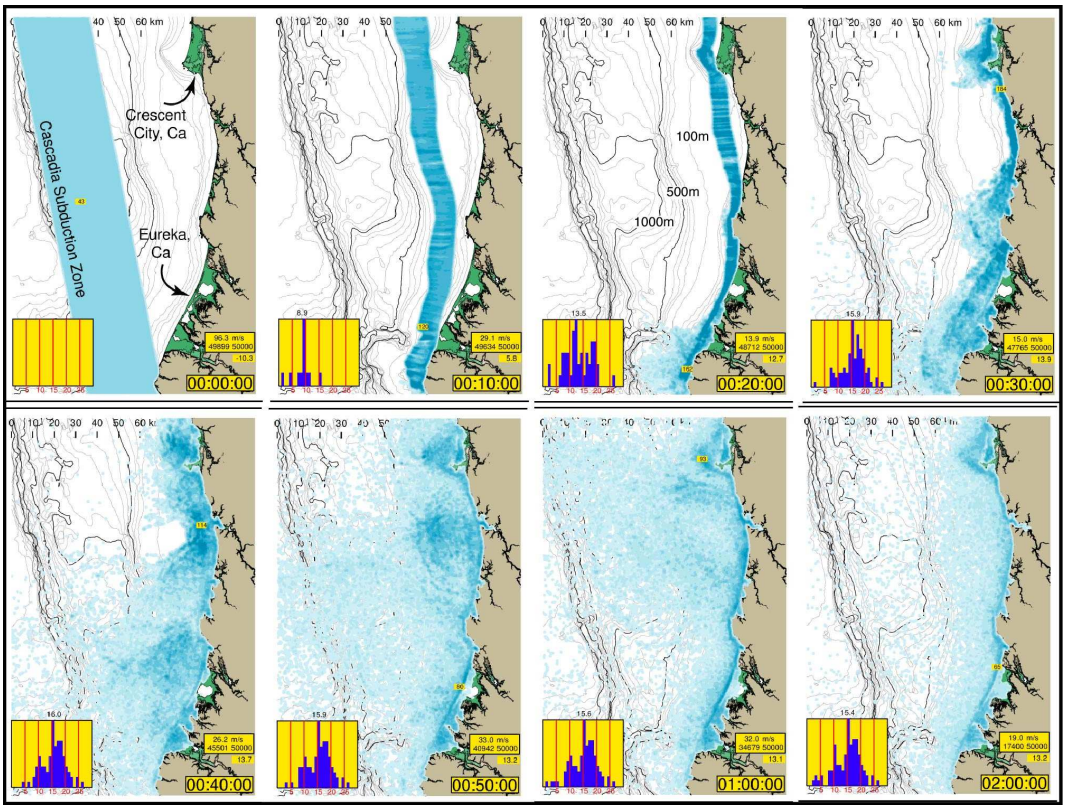

Figure 11: Northern California tsunami inundation simulation. This scenario supposes that a Cascadia mega-thrust earthquake sends a 4m wave landward from the trench. Note the strong reflections from the steep headlands and the flooding of the lowlands. The yellow box at lower left shows the statistical distribution of runup heights along the coast. Bold contours are 500m.

4.2 Northern California–a Cascadia earthquake tsunami

In United States' Pacific Northwest, a major tsunami hazard lurks in the Cascadia subduction zone just to the west of the continent. The next Cascadia mega-thrust earthquake (∼M9) might slip the zone 15-20m and uplift the seabed east of the trench by several meters. Fig. 11 pictures a 60,000 tsunami ball simulation of runup and inundation of northern California for a plausible Cascadia earthquake scenario.

Like the Babi Island example, a uniform 4m high, 35km wide (360s period in this water depth) wave is sent toward the California coast. The i-th ball starts with a rightward velocity of $\sqrt{gH(\mathbf{r}_0^i)}$ where $\mathbf{r}_0^i$ is its initial position. To 100m depth, slope here measures 1:150 to 1:250. Green's Law (3.2) says that a 4m wave starting at 1000m depth should have amplitude $4(1000/95)^{0.25}=7.1$m at 95m. Given an offshore height to offshore depth ratio there of ∼0.07, a beach slope of $\sim 0.5^\circ$, and a period of 360s, the center of Fig. 8 predicts that on a plane beach the wave should run up ∼2.8 times its height at 95m depth, or 19.9m.

Unlike the Babi Island example, real offshore and onshore topography is ragged. Tsunami balls, accelerating in proportion to the gradient of topography, take on a random walk component. Even before striking shore, ray theory refraction of balls grazing steep slopes generates streaks of concentrated and diffused energy (Panels 2-3, Fig. 11). Small changes in wave incident direction move these streaks around in an unpredictable fashion.

Upon beaching, those balls contacting steep topography bounce off in coherent reflections whereas those balls meeting coastal flats or drainages rush inland. Many of the reflected balls become trapped in littoral drift, striking the coast repeatedly as their paths rotate toward shallow water. Some of the balls that rushed inland become stalled behind low coastal hills and dunes. Bits of tsunami persist to six hours and more. Like much of California, the steep coastline here limits tsunami run-in to isolated flatlands and drainages. Of course, major populations often center at such locations–e.g. Eureka and Crescent City. If a Cascadia earthquake were to send in a 4m wave as modeled, we predict runups between 4m and 27m with a mean of 15.4m. Full runup statistics (yellow box inset of Fig. 11), in addition to likelihood estimates that a Cascadia earthquake were to send in a 4m wave versus a 3m one, versus 2m one etc. form a sound basis for probabilistic tsunami hazard analysis. Click here Humbolt-in2x.mov and Humbolt-in2.mov for Quicktime versions of Fig. 11.

4.3 Southeast United States–A La Palma wave

Fig. 12 stages a runup and inundation simulation for the southeast United States. The coasts of Florida, Georgia and South Carolina present a contrasting tsunami environment to Northern California. On one hand, the southeast coast has a wide and shallow continental shelf. Water sounds to 30m depth and less out to 60km from shore (1:2600 slope). Judging from the two dimensional simulations, large steep waves in this environment may break far from the beach. On the other hand, 10m elevations onshore are not topped for 60km inland and many wide waterways deeply penetrate the coast. Tsunami that do reach the shore face few obstacles to minimize run in.

No subduction zone exists off the east coast of the United States, so earthquake tsunami here are rare and small. Potential landslide tsunami sources however, do exist in the Atlantic basin. Ward and Day (2000) present evidence that Cumbre Vieja Volcano on La Palma Island is in the later stages of a growth/collapse cycle that will climax in a flank failure involving as much as 500 km^3 of material. Their simulations predict that a high speed landslide of this volume might fling dozens of 20m high, 10 minute period waves toward the U.S. East Coast.

Fig. 12 pictures a 100,000 tsunami ball simulation of runup and inundation from a single 10m high, 35km wide, 660s period, La Palma wave. The i-th ball starts with a rightward velocity of $\sqrt{gH(\mathbf{r}_0^i)}$ where $\mathbf{r}_0^i$ is its initial position. Green's Law (3.2) says that a 10m wave starting at 200m depth should have amplitude $10(200/50)^{0.25} = 14$m at 50m.

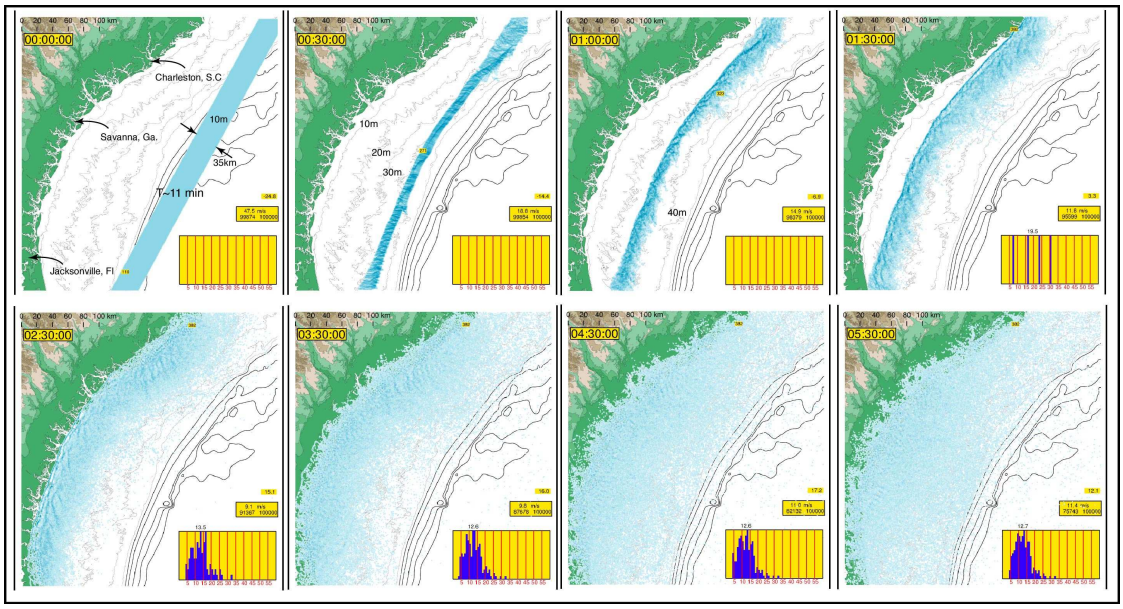

Figure 12: Runup and inundation of Southeast U.S.A. from a single 10m high, 660s period tsunami parented by a La Palma Island collapse. Run in across the lowland extends 30-50km. Thin and bold contours offshore are 10 m and 100m.

Given an offshore height to offshore depth ratio there of $\sim$0.28, a beach slope of $\sim 0.011^\circ$, and a period of 660s, the left frame of Fig. 8 predicts run up $\sim$1.1 times wave height at 50m depth, or 15.4m. Actual slopes (1:2600) fall considerably short of 1:520 so the 15.4m estimate is probably high. Wave breaking commences 60 km out and has 1-2 hours to act (Panel 2 Fig. 12). The wave spreads and some balls turn back before the wave reaches land (Panels 3-6). Note the lack of reflections, the flat coast acts like a tsunami absorber. When all is said and done, run up averaged 12.6m with a large spread. Run in across the lowland extends 30-50km.

Run up amplification in Fig. 12 hardly exceeded one, so the shallow shelf adjacent to the Southeast U.S. does offer a modicum of protection from a 10m, 660s La Palma wave. Still, Ward and Day (2006) forecast a great sequence of waves from a La Palma landslide, not just one. Recalling the effect of wave set up (Fig. 9), likely flooding will be more extensive than pictured. Click here Savanna-10.mov and here Savanna-10-num.mov for a Quicktime versions of Fig. 12.

5 Runup as a statistical quantity

The three dimensional simulations in Figs. 11 and 12 input waves of uniform height, yet runup varied widely. The spread finds origin both offshore and onshore: (a) Peculiarities of offshore bathymetry concentrate or disperse tsunami energy in deep water. (b) Peculiarities in wave breaking toss tsunami balls onto land with different speeds and turn

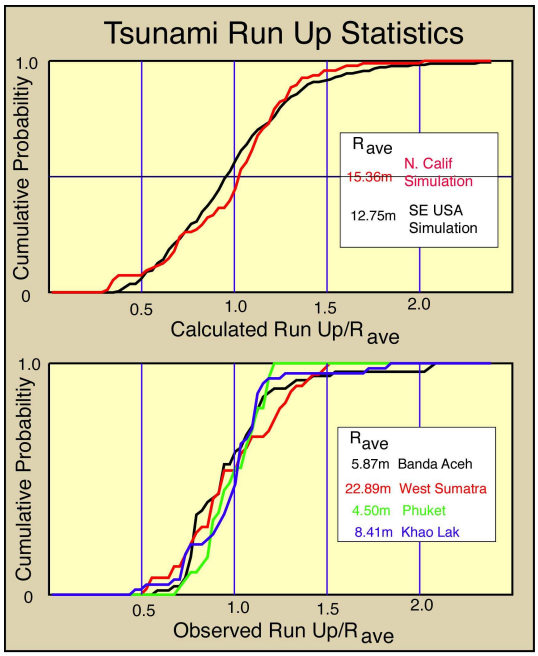

Figure 13: (Top) Cumulative distribution of run up values from the simulations of Figs. 11 and 12 normalized to their mean value. (Bottom) 2004 observed normalized runup distributions from four sites in Thailand and Sumatra. Normalized runup may have the same statistical behavior everywhere.

back others. (c) Peculiarities of onshore topography funnel water or overlap reflections. (d) Of course too, some shoreline sites are just more sheltered than others. Even in these fully deterministic calculations, minor changes in initial wave conditions play through to substantial changes in runup locally. Because such variations also occur in nature, constructing single valued inundation hazard maps is fruitless. We believe that the only meaningful description of runup is in terms of a random process. The best that one can hope for in describing a random process is to characterize its statistical properties. Of these, mean and variance about the mean head the list.

Fig. 13 (top) plots cumulative distribution of runup heights from the Northern California and Southeast U.S. inundation simulations normalized to their mean values. Although conditions for the two cases were markedly different, both distributions trend similarly–spreading to about 1/2 to 2 times the mean value. Fig. 13 (bottom) plots cumulative probability of runup height from the 2004 Sumatra tsunami at Banda Aceh, West Sumatra, Phuket and Khao Lak as summarized from post-event surveys (Matsutomi et al., 2005; Sato et al., 2005; Tsuji et al., 2005). These four locations too, separate widely geographically and in mean wave height, but the normalized run up distributions nearly overlap. Although our analysis is cursory, we speculate that normalized runup may have the same statistical behavior everywhere. If so, a single estimate of mean would fully characterize runup statistics. Such a finding would greatly simplify probabilistic hazard estimation by obviating the need for detailed tsunami simulations at every location.

6 Conclusions

This paper develops a new, granular approach to the "last mile" problem of tsunami runup and inundation. The grains employed here are not fluid, but bits, or balls, of tsunami energy. By careful formulation of the ball accelerations, both wave-like and flood-like behaviors are accommodated so tsunami waves can be run seamlessly from deep water, through wave breaking, to the final surge onto shore and back again. In deep water, tsunami balls track according long wave ray theory. On land, tsunami balls behave like a water landslide. In shallow water, the balls embody both deep water and on land elements. Tsunami balls offer a competitive alternative to traditional run up models. The tsunami ball approach applies to any environment (defended harbors, lakes, fiords) where non-dispersive ray theory describes deep water wave propagation.

The introduction of self-topography to tsunami ball accelerations mimics flood-like behaviors on land. Off shore, self-topography induces breaking that limits subsequent inundation by disrupting inbound waves. Consequences of breaking are complex and depend on the wave period, wave amplitude, wave shape and beach slope.

When applied to two-dimensional single waves of 50-1100s period on 1:100-1:500 beaches, we find that runup amplification increases with beach slope and wave period and decreases with input wave amplitude. These trends coincide with laboratory results, but few wave tank experiments approach the low slopes and long wavelengths needed to make a quantitative comparison.

Tsunami ball simulations predict that only a portion of the wave sent to the beach actually reaches shore. Much of the water piles up, then returns to sea as reverse breakers prior to peak run up. When tsunami consist of many waves, the pile-up grows in duration and size and slowly floods the land as set up.

When applied to three-dimensional geometries, we find that the two-dimensional results generally hold, although runup values widely scatter due to complications of wave refraction and interference. Two cases employing real topography–a steep California coast and a flat Georgia coast–highlight the practical elegance of the tsunami ball approach. A 4m wave sent onto the California coast from a Cascadia earthquake averages 15.4m runup. In contrast, a larger 10m La Palma wave directed to the Georgia coast runs up just 12.7m on average. Georgia's adjacent wide shallow continental shelf provides a bit of protection from steep, large amplitude tsunami in the form of a lower runup amplification. Conversely, Georgia's flat coastal terrain and penetrating watercourses offer no resistance to run in, once tsunami reach shore.

Because of their highly non-linear nature, we argue that runup and inundation are best considered to be random processes rather than deterministic ones. Models and observations hint that for uniform input wave conditions, normalized runup statistics everywhere follow a single skewed distribution with a spread between 1/2 and 2 times its mean.

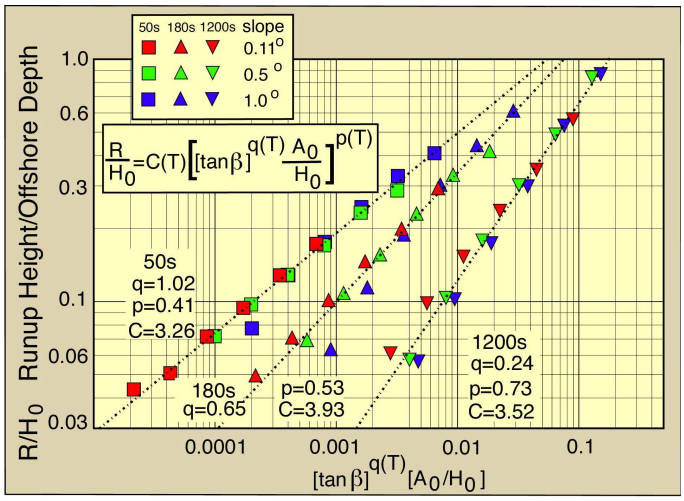

Figure 14: Summary of tsunami ball runup experiments in Fig. 8 weighted by $\tan\beta$ to the power q. Exponent q decreases with increasing wave period.

Appendix A: Separation of slope and period effects on the runup of single waves

By plotting the results of Fig. 8 weighted by $(\tan\beta)^q$, the influences of beach slope and wave period on the runup of single waves separate nicely (Fig. 14). Best-fit q-exponents decrease consistently with increasing wave period. Moreover, the uniform increase in slope of the least square fits in Fig. 14 suggest a runup law of the form

$$\frac{R}{H_0} = C(T)\left[(\tan\beta)^{q(T)}\frac{A_0}{H_0}\right]^{p(T)} \tag{A.1}$$

or

$$\frac{R}{A_0} = C(T)(\tan\beta)^{q(T)p(T)}\left[\frac{A_0}{H_0}\right]^{p(T)-1}, \tag{A.2}$$

with

$$\begin{aligned} &C(50)=3.26; \quad q(50)=1.02; \quad p(50)=0.41;\\ &C(180)=3.93; \quad q(180)=0.65; \quad p(180)=0.53;\\ &C(1200)=3.52; \quad q(1200)=0.24; \quad p(1200)=0.73. \end{aligned}$$

Fig. 15 plots (A.1) for the three periods above for slopes of 1° (top) and 2.88° (bottom). The latter 1:19.85 slope, three times steeper than any case examined here, corresponds to the shallowest slope experiment run by Synolakis (1986). The dots in the bottom panel indicate relative runup heights of breaking solitary waves measured by Synolakis (1986)

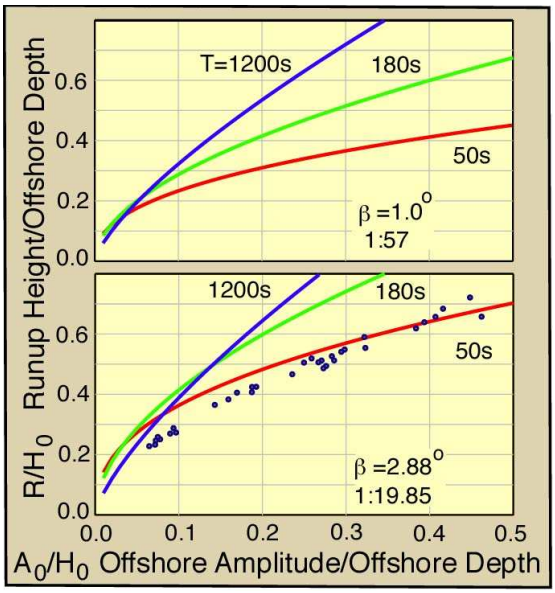

Figure 15: Relative runup predicted for beach slopes of 1° and 2.88° for three wave periods. Experimental observations of breaking solitary wave runup are shown by the dots in the lower panel.

as reported in Li and Raichlen (2002). Solitary waves in the Synolakis experiments have cross sectional shapes

$$A(x) = (A_0/H_0)\,\mathrm{sech}^2\left[\sqrt{\frac{3A_0}{4H_0}}x\right] \tag{A.3}$$

and pulse widths of about $5/(A_0/H_0)^{1/2}$ times the offshore depth. In our experiments $H_0 = 100$m, so the equivalent wave widths of (A.2) have durations (15.8)(100m)/(9.8m/s^2 100m)$^{1/2}\sim$50s for (A_0/H_0)=0.1 and (7.1)(100m)/(9.8m/s^2 100m)$^{1/2}\sim$23s for (A_0/H_0)=0.5. Roughly then, the red line in the bottom panel of Fig. 15, corresponds to the wave lengths of the Synolakis (1986) experiment. As yet, we have made no specific attempt to "tune" the tsunami ball process to reproduce laboratory data. Judging from the fairly good fit in Fig. 15, the tsunami ball approach even as it is now, seems to capture many of the breaking wave behaviors exposed in experiment.

Lastly, note that runups for the 1200s waves are only weakly dependent on beach slope in the range (0.11° to 1°). A simplified runup formula for long period earthquake tsunami waves that ignores beach slope variations might take the form

$$\begin{aligned} &R/H_0 = 1.5(A_0/H_0)^{0.7} \quad \text{or} \quad R/A_0 = 1.5(A_0/H_0)^{-0.3}, \\ &A_0 < (H_0/2) \ll \lambda_0; \quad H_0 = 100\text{m}. \end{aligned} \tag{A.4}$$

Contrast (A.4) with (3.4). Eqs. (A.1), (A.2) and (A.4) apply to 100m water depths and $A_0 < H_0/2$. For other starting conditions A_0', H_0' and $A_0' < H_0'/2$, replace A_0 by $A_0'[H_0'/H_0]^{1/4}$.

Figure 16: Frames taken from a yacht at anchor off Phi Phi Island Thailand during the initial on shore flow stage of the December 26th 2004 tsunami. Note the reverse facing and traveling breakers turned back from a near shore water pile up similar to that predicted here http://es.ucsc.edu/∼ward/RU(1200s-20m-0.5).mov See-http://www.yachtaragorn.com/Thailand.htm

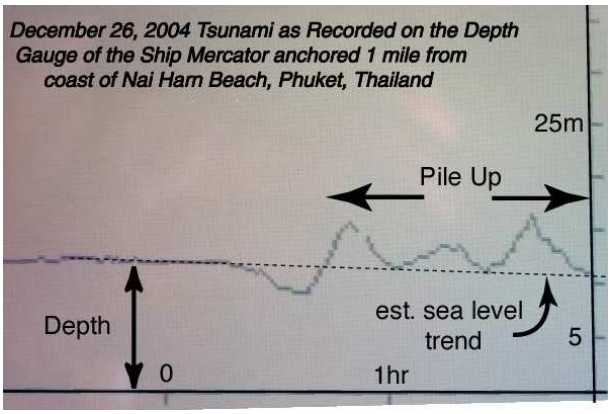

Figure 17: Depth Gauge recording from the ship Mercator. After the initial draw down, several wave crests and troughs came by, but the water depth never fell below the pre-tsunami level. We believe that the ship was riding on a water pileup. From: http://www.zeilen.com/publish/article_1659.shtml

Below are several 2-D and 3-D runup and inundation movies computed using tsunami ball theory.

In this article:

http://es.ucsc.edu/∼ward/RU(50s-20m-0.11).mov
http://es.ucsc.edu/∼ward/RU(180s-20m-0.11).mov
http://es.ucsc.edu/∼ward/RU(1200s-20m-0.11).mov
http://es.ucsc.edu/∼ward/RU(1200s-20m-0.5).mov
http://es.ucsc.edu/∼ward/RU(180s-20m-0.11)set.mov
http://es.ucsc.edu/∼ward/Babi.mov
http://es.ucsc.edu/∼ward/Babi-num.mov
http://es.ucsc.edu/∼ward/Humbolt-in2x.mov
http://es.ucsc.edu/∼ward/Humbolt-in2.mov
http://es.ucsc.edu/∼ward/Savanna-10.mov
http://es.ucsc.edu/∼ward/Savanna-10-num.mov

Others:

http://es.ucsc.edu/∼ward/RU(25s-5m-0.11).mov
http://es.ucsc.edu/∼ward/RU(25s-5m-0.11+3).mov
http://es.ucsc.edu/∼ward/RU(25s-5m-0.11-3).mov
http://es.ucsc.edu/∼ward/RU(180s-5m-0.11).mov
http://es.ucsc.edu/∼ward/RU(180s-5m-0.11+3).mov
http://es.ucsc.edu/∼ward/RU(180s-5m-0.11-3).mov
http://es.ucsc.edu/∼ward/RU(1200s-5m-0.11).mov
http://es.ucsc.edu/∼ward/RU(1200s-5m-0.11+3).mov
http://es.ucsc.edu/∼ward/RU(1200s-5m-0.11-3).mov
http://es.ucsc.edu/∼ward/Lituya-2D.mov
http://es.ucsc.edu/∼ward/shoreline-2.mov
http://es.ucsc.edu/∼ward/mont-bay.mov
http://es.ucsc.edu/∼ward/SFO.mov
http://es.ucsc.edu/∼ward/c-cod-final.mov

References

[1] M. J. Briggs, C. E. Synolakis, G. S. Harkins and D. Green, Laboratory experiments of tsunami runup on a circular island, Pure Appl. Geophys., 144 (1994), 569-593.
[2] M. J. Briggs, C. E. Synolakis, G. S. Harkins and S. A. Hughes, Large scale three dimensional experiments of tsunami inundation, in: Y. Tsuchiya and N. Shuto (Eds.), Tsunami: Progress in Prediction, Disaster Prevention and Warning, Kluwer, Boston, 1995, pp. 129-149.
[3] S. R. Chesley and S. N. Ward, Impact-generated tsunami: A quantitative assessment of human and economic hazard, J. Nat. Hazards, 38 (2006), 355-374.
[4] Y. Y. Chao, The theory of wave refraction in shoaling water, including the effects of caustics and the spherical earth, New York University, School of Engineering and Science, University Heights New York, 1970, 10453.

[5] M. Herrmann, Two-phase flow, 2006 CTR summer program tutorial, 2006, http://www.stanford.edu/group/ctr/
[6] S. Hibberd and D. H. Peregrine, Surf and run-up on a beach: a uniform bore, J. Fluid Mech., 95 (1979), 323-345.
[7] A. B. Kennedy, Q. Chen, J. T. Kirby and R. A. Dalrymple, Boussinesq modeling of wave transformation, breaking, and run-up. Part I: 1D, J. Waterw. Port C.-ASCE, 126(1) (2000), 39-47.
[8] B. Le Mehaute and S. Wang, Water Waves Generated by Underwater Explosions, World Scientific, New Jersey, 1996.
[9] Y. Li and F. Raichlen, Non-breaking and breaking solitary wave run-up, J. Fluid Mech., 456 (2002), 295-318.
[10] P. L. Liu, Y. S. Cho, M. J. Briggs, U. Kanoglu and C. E. Synolakis, Runup of solitary waves on a circular island, J. Fluid Mech., 320 (1995), 259-285.
[11] P. J. Lynett, T.-R. Wu and P. L.-F. Liu, Modeling wave runup with depth-integrated equations, Coast. Eng., 46 (2002), 89-107.
[12] H. Matsutomi et al., The December 26, 2004 Sumatra Earthquake Tsunami, Tsunami Field Survey around Phuket, Thailand, 2005, http://www.drs.dpri.kyoto-u.ac.jp/sumatra/thailand/phuket_survey_e.html
[13] D. H. Peregrine, Calculations of the development of an undular bore, J. Fluid Mech., 35 (1966), 321-330.
[14] S. Sato et al., 2004 Sumatra Tsunami, Survey around South Part of SriLanka, 2005, http://www.drs.dpri.kyoto-u.ac.jp/sumatra/srilanka-ut/SriLanka_UTeng.html
[15] C. E. Synolakis, The run up of solitary waves, J. Fluid Mech., 185 (1986), 523-545.
[16] C. E. Synolakis and E. N. Bernard, Tsunami science before and beyond Boxing Day 2004, Philos. T. Roy. Soc., 364 (2006), 2231-2265.
[17] V. V. Titov and C. E. Synolakis, Modeling of breaking and non-breaking long-wave evolution and runup using VTCS-2, J. Waterw. Port C.-ACSE, 121 (1995), 308-316.
[18] V. V. Titov and C. E. Synolakis, Numerical modeling of tidal wave runup, J. Waterw. Port C.-ACSE, 124 (1998), 157-171.
[19] Y. Tsuji et al., The 26 December 2004 Indian Ocean Tsunami: Initial Findings from Sumatra, 2005, http://walrus.wr.usgs.gov/tsunami/sumatra05/index.html
[20] S. N. Ward and S. Day, Cumbre Vieja Volcano–Potential collapse and tsunami at La Palma, Canary Islands, Geophys. Res. Lett., 28 (2001), 3397-3400.
[21] S. N. Ward and S. Day, A particulate kinematic model for large debris avalanches: Interpretation of debris avalanche deposits and landslide seismic signals of Mount St. Helens, May 18th 1980, Geophys. J. Int., 167 (2006), 991-1004.